| | Conventional $TiO_2$ | Superporous $TiO_2$ | Anatase |
|---|---|---|---|
| $R_{WP}$ [%] | 1.44 | 1.61 | 5.08 |
| $R_I$ [%] | 2.32 | 4.47 | 2.91 |
| | | | |
| a [Å] | 3.78556(4) | 3.7869(1) | 3.78509(1) |
| c [Å] | 9.5046(1) | 9.4812(4) | 9.51264(4) |
| V [$Å^3$] | 136.205(4) | 135.96(1) | 136.287(1) |
| | | | |
| $z_O$ | 0.20808(2) | 0.20792(4) | 0.20792(3) |
| $B_{Ti}$ [$Å^2$] | 0.547(3) | 0.366(5) | 0.477(5) |
| $B_O$ [$Å^2$] | 0.97(1) | 1.39(2) | 0.80(1) |
| | | | |
| Ti-O [Å] | 1.9777(2) | 1.9713(5) | 1.9779(3) |
| Ti-O' [Å] | 1.93426(6) | 1.9350(1) | 1.93441(6) |
| ∠O-Ti-O [°] | 101.887(6) | 101.90(1) | 101.943(8) |
| ∠O-Ti-O' [°] | 92.432(2) | 92.436(5) | 92.454(3) |

**Supplementary Table 1.** Rietveld analysis of conventional $TiO_2$, superporous $TiO_2$, anatase powders.

In the Rietveld analysis, the ion positions and isotropic temperature factors were adopted as structural fitting parameters. Table S1 shows the coordinated structural parameters and reliability factors $R_{WP}$ and $R_I$ from this analysis.

Although main crystal phase of the two samples was anatase, however, the lattice constant *a* decreased in the order of superporous $TiO_2$, conventional $TiO_2$ and the reference anatase.

In contrast, lattice constant *c* increased in the same order. In anatase $TiO_2$ (space group $I4_1/amd$), the oxygen atoms are free to move only in the z direction. On determining the $z_0$ values and temperature factors $B_{Ti}$ and $B_O$ of titanium and oxygen, some differences can be seen in the three samples. However, given the small crystallite sizes of the samples, and concomitant broad Laue functions and XRD peaks, the differences appear to be within the experimental uncertainty.

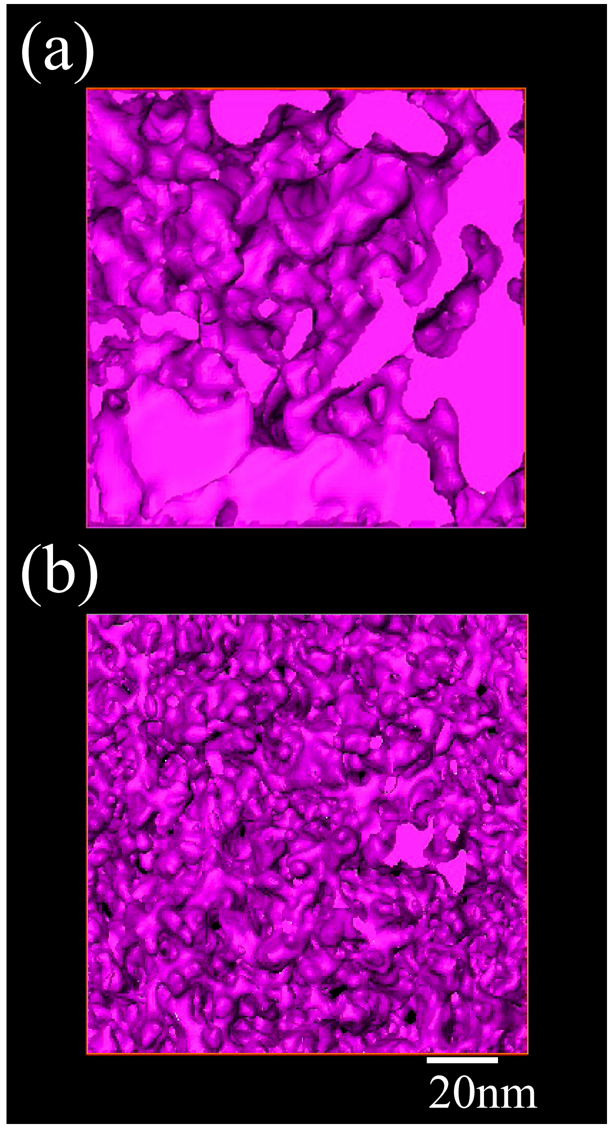


**Supplementary Figure 1.** Reconstructed surface rendering images of the conventional $TiO_2$ (a) and the superporous $TiO_2$ (b). The voxel images are encoded using a drawing software (amira®, Visage Imaging Co.). The animated rotating images are also available for inspection at http://sirius.esi.nagoya-u.ac.jp/~tanakalab/yoshida/MicroscopyandMicroanalysis/2010.html.

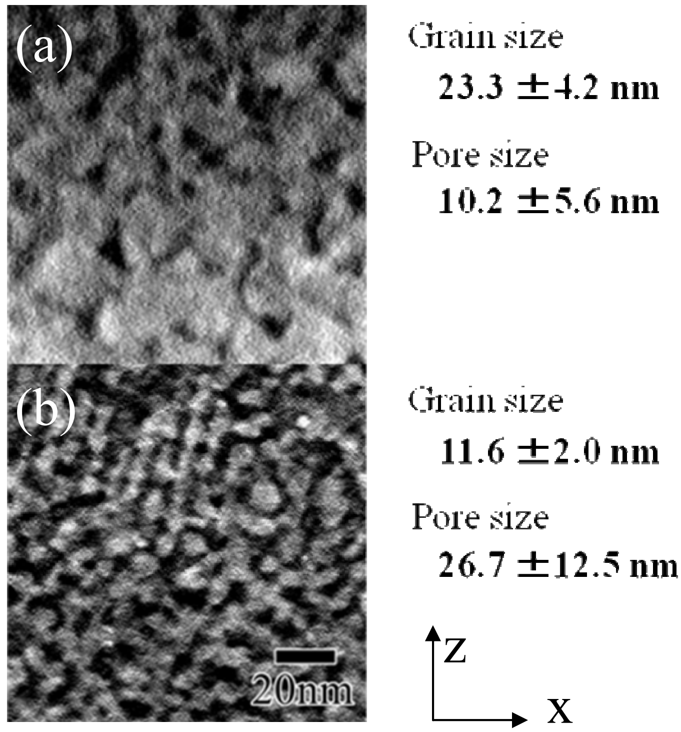


**Supplementary Figure 2.** Y(x-z) sliced images and 3 dimensionally estimated grain sizes and pore sizes of the conventional $TiO_2$ (a) and the superporous $TiO_2$ (b).

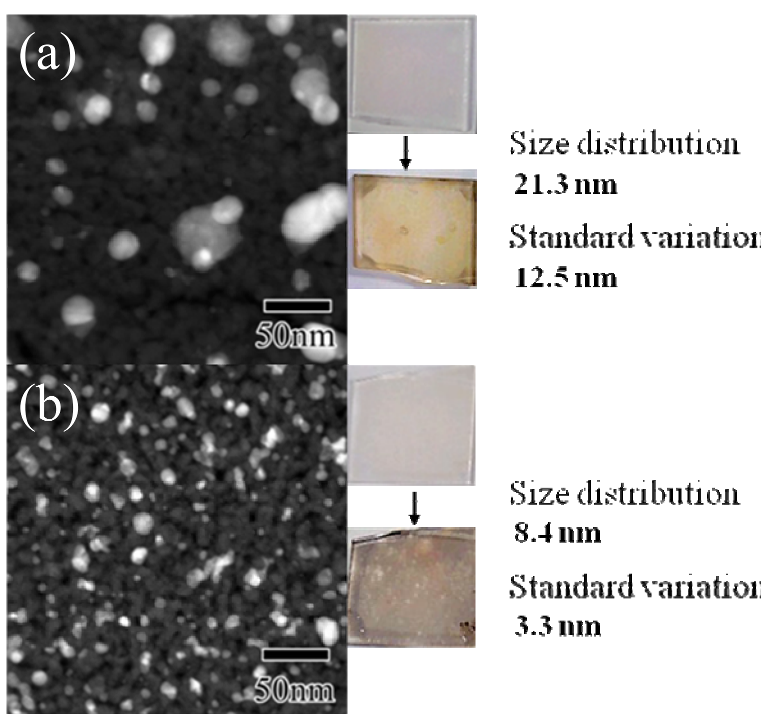


**Supplementary Figure 3.** Low-magnification HAADF-STEM images and photographs of Ag/conventional $TiO_2$ (a) and Ag/superporous $TiO_2$ (b).

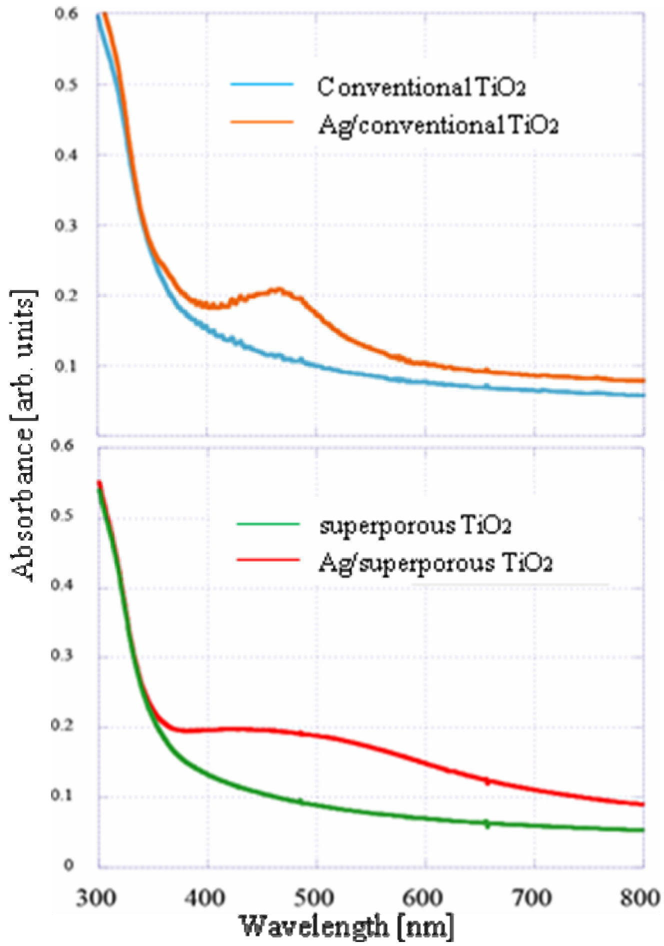


**Supplementary Figure 4.** UV-Vis absorption spectra taken before/after participation on the conventional $TiO_2$ and superporous $TiO_2$.

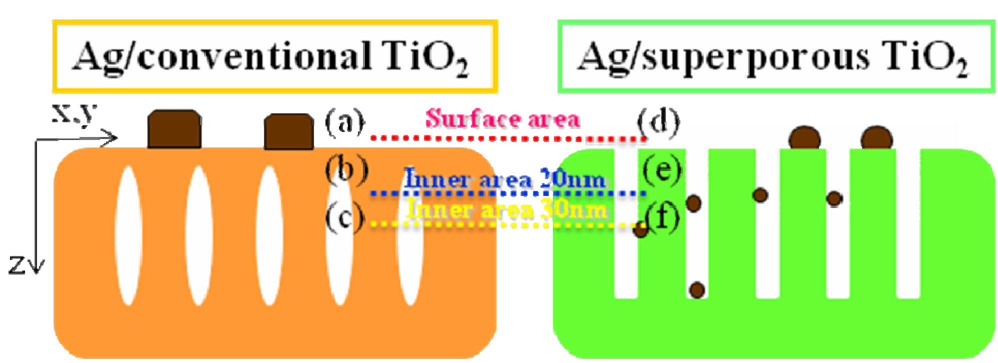


**Supplementary Figure 5.** Schematic diagram showing positions of Z slice images indicated in Figure 7.

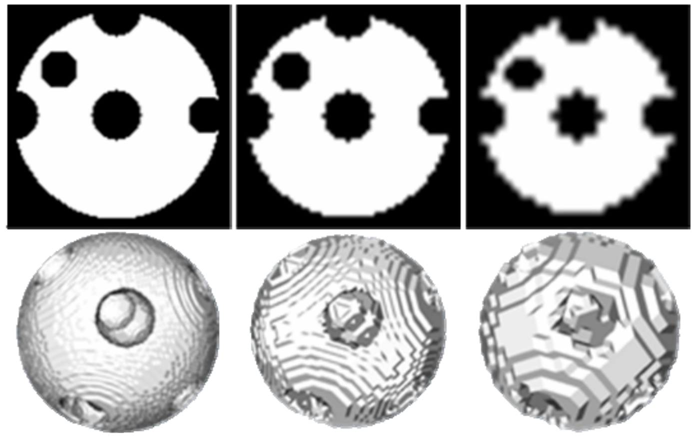

**Supplementary Figure 6.** Schematic diagram of 3D reconstruction and rendering error of discrete object.

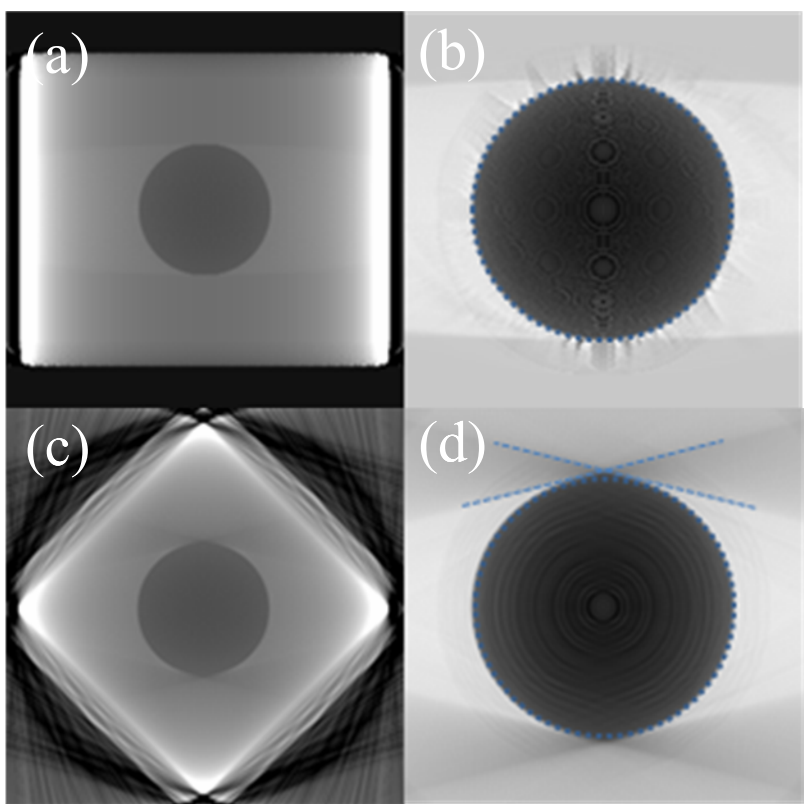


**Supplementary Figure 7.** Simulation of reconstruction error (Model: a sphere of 256 pixel in 700×512×512 cuboid). ±75 degree single tilt with 1 degree step. Z (x-y) slice image (a) and magnified image (b). Y (x-z) slice image (c) and magnified image (d).